Expression and purification of the extracellular domain of wild-type humanRET and the dimeric oncogenic mutant C634R

Liu, Yixin

2020-12-01

Liu , Y , Ribeiro , O D C , Robinson , J & Goldman , A 2020 , ' Expression and purification of the extracellular domain of wild-type humanRET and the dimeric oncogenic mutant C634R ' , International Journal of Biological Macromolecules , vol. 164 , pp. 1621-1630 . https://doi.org/10.1016/j.ijbiomac.2020

http://hdl.handle.net/10138/332918
https://doi.org/10.1016/j.ijbiomac.2020.07.290

Expression and purification of the extracellular domain of wild-type humanRET and the dimeric oncogenic mutant C634R

Yixin Liu[1], Orquidea De Castro Ribeiro[1], James Robinson[2], and Adrian Goldman[1,3*]

[1] Molecular and Integrative Biosciences, Faculty of Biological and Environmental Sciences, University of Helsinki, Helsinki 00790, Finland.

[2] Discovery and Translational Sciences Department, Leeds Institute of Cardiovascular and Metabolic Medicine, School of Medicine, University of Leeds, Leeds LS2 9JT, U.K.

[3] Astbury Centre for Structural Molecular Biology, School of Biomedical Sciences, University of Leeds, Leeds LS2 9JT, U.K.

*To whom correspondence should be addressed:

[3] Astbury Centre for Structural Molecular Biology, School of Biomedical Sciences, University of Leeds, Leeds LS2 9JT, U.K. a.goldman@leeds.ac.uk

Abstract

The receptor tyrosine kinase RET is essential in a variety of cellular processes. RET gain-of-function is strongly associated with several cancers, notably multiple endocrine neoplasia type 2A (MEN 2A), while RET loss-of-function causes Hirschsprung's disease and Parkinson's disease. To investigate the activation mechanism of RET as well as to enable drug development, over-expressed recombinant protein is needed for *in vitro* functional and structural studies. By comparing insect and mammalian cells expression of the RET extracellular domain (RET^{ECD}), we showed that the expression yields of RET^{ECD} using both systems were comparable, but mammalian cells produced monomeric functional RET^{ECD}, whereas RET^{ECD} expressed in insect cells was non-functional and multimeric. This was most likely due to incorrect disulfide formation. By fusing an Fc tag to the C-terminus of RET^{ECD}, we were able to produce, in HEK293T cells, dimeric oncogenic RET^{ECD} (C634R) for the first time. The protein remained dimeric even after cleavage of the tag via the cysteine disulphide, as in full-length RET in the context of MEN 2A and related pathologies. Our work thus provides valuable tools for functional and structural studies of the RET signalling system and its oncogenic activation mechanisms.

Key words

receptor tyrosine kinase, recombinant protein expression, cysteine-rich domain

Funding: This work was supported by the Centre for International Mobility (CIMO, TM-16-10170) to AG and YL; the European Molecular Biology Organization (No. 8476) to YL; the Academy of Finland (No. 322609) to AG; the Academy of Finland (No. 286429) to AG; and the Biotechnology and Biological Sciences Research Council (BBSRC, BB/M021610/1) to AG.

1. Introduction

Re-arranged during transfection (RET) receptor tyrosine kinase is a single-pass transmembrane protein that is important in multiple cellular processes including cell migration, proliferation, differentiation and maintenance [1–3]. RET is a versatile receptor tyrosine kinase that interacts through a co-receptor with four glial-cell-line-derived neurotrophic factor (GDNF) ligands of the TGF-β superfamily (collectively, GFLs), GDNF, neurturin (NTRN), artemin (ARTN) and persephin (PSPN) as well as growth and differentiation factor 15 (GDF15), which is a distant relative of the GFLs [4–12]. RET has an extracellular domain (ECD) comprised of four cadherin-like domains (CLDs) and a cysteine-rich domain (CRD). Cryo-electron microscopy (cryo-EM) structures of RET in complex with its ligands show that the complex of dimeric GDNF ligands and co-receptors recruits two molecules of RET to form a 2:2:2 C-clamp shaped complex. The RET ECD interacts with the co-receptors through its N-terminal domain and with the GDNF ligands through its C-terminal end; and correct folding and intermolecular interaction also requires the binding of calcium ions at CLD2-3 [13–17] and possibly in the CRD as well [16]. RET^{CRD} contains eight intramolecular disulfide bonds and exhibits a unique fold [16]. This is then followed by a transmembrane domain, an intracellular juxtamembrane region and a tyrosine kinase domain. RET signaling is mediated by binding of GFLs and GDF15 to their corresponding GDNF receptors (GFRα1-4) or GDNF receptor-like (GFRAL), forming a complex that recruits RET to form an active heterohexameric complex that leads to the activation of RET at the tyrosine kinase domain for downstream cell signaling [15–17].

Mutations in RET lead to a variety of human diseases. For example, gain-of-function mutations are strongly associated with cancers, including non-small-cell cancer (NSCC) and MEN 2A, while loss-of-function mutations contribute to Parkinson's disease and Hirschsprung's disease [1–3]. In the case of MEN 2A, point mutations of the cysteine residues in the CRD, most commonly C634R, lead to ligand-independent receptor activation [18,19]. In wild-type RET, C634 forms an intramolecular disulfide bond with C630 and, as a result, the oncogenic C634R mutation leaves C630 unpaired such that it can form intermolecular disulfide bonds [15,17]. The commonly accepted mechanism of activation is that C630 cross-links two RET molecules together via a C630-C630 disulfide bond, facilitating autophosphorylation and activation of the intracellular

kinase domain (**Fig. 1**). However, previous reports suggested recombinantly expressed ECD of RET^{C634R} mutant did not form a RET homodimer [15,20].

Considering their clinical importance, RET and its complexes, as well as its oncogenic mutants, represent valid therapeutic targets. The FDA have approved a number of inhibitors targeting the intracellular domain of RET, such as cabozantinib, lenvatinib and selpercatinib for cancers associated with RET fusions or oncogenic mutations [21]. All of the approved inhibitors target multiple receptor tyrosine kinases (RTKs) due to the conservation of the intracellular kinase domain among different RTKs such as Trk and vascular endothelial growth factor (VEGF) receptors [22]. Therefore, drugs that specifically targeting RET^{ECD} or its complexes would have improved specificity and, presumably, fewer side-effects.

To produce sufficient functional proteins for structural determination, eukaryotic proteins have been expressed recombinantly in a variety of expression hosts, including bacteria, yeast, insect cells and mammalian cells. The optimal host to use for protein over-expression is largely protein dependent. For the EGFR [23–26], Eph [27–29] and Trk [30] RTKs, the extracellular domains or full-length receptors have been successfully expressed in both insect and mammalian expression systems. However, only mammalian cell expression, including CHO and HEK cells, has been reported to be successful for recombinant humanRET to generate protein for functional and structural studies [15–17,20,31]. On the other hand, baculovirus-infected insect cells have two advantages over mammalian cells: cost-efficiency and ease of large-scale expression. Moreover, insect cells are also capable of producing posttranslational modifications (PTMs), for instance, glycosylation, which is important for the folding and signaling of RTKs [32], making it a powerful system for recombinant eukaryotic protein expression.

In the current study, we used both insect and mammalian cell expression systems to express the extracellular domain (ECD) of humanRET to investigate the impact of expression hosts on its function and describe the first overexpression and purification of the dimeric form of the extracellular domain of RET (C634R).

2. Materials and methods

2.1 Constructs

All the constructs used in this study are summarized in **Table 1**. For RET expression in mammalian cells with its native signal peptide, wild-type humanRET^{ECD} (residues 1-635) and the mutants (C634R, C86R, C216S) were sub-cloned into pcDNA3.1 vector with a C-terminal Tobacco Etch Virus (TEV) protease cleavage site and His_8-Flag (HF) tags. When Igκ and CD33 signal peptides were used, the mature wild-type humanRET^{ECD} (residues 28-635) was cloned into the vector with the same protease site followed by either a His_8 (H) or HF tags. HumanRET^{ECD}-Fc harbouring the C634R (RET^{C634R}-Fc) and C634R, C86R, C216S (RET^{C634R*}-Fc) mutations were cloned into the same vector with C-terminal HF tags. Additionally, a G_4S linker was cloned between the TEV protease cleavage site and the Fc tag in two of the RET$^{C634R(*)}$-Fc contructs.

Mature humanGDF15 (residues 195-308) preceded by an N-terminal modified Fc tag with a thrombin cleavage site was cloned into the pcDNA3.1 vector, and a modified Fc protein [33,34] was cloned into the pIRES-eGFP vector. Both the Fc and Fc-GDF15 expression constructs use the Igκ signal peptide for protein secretion and were used for co-expression. For RET expression in insect cells, wild-type humanRET^{ECD} (28-635) was sub-cloned into a pK503.9 vector (modified from pFastBac vector) [35] with N-terminal Flag-His_8 (FH) tags and a thrombin cleavage site. HumanGFRAL^{ECD} (residues 19-351) with a C-terminal TEV cleavage site and His_8-twin Strep (HS) tags was cloned into pK503.9 vector and is referred to as GFRAL in this study.

2.2 Cell culture and protein expression

An adherent culture of HEK293T cells (American Type Culture Collection, CRL-3216) was maintained in Dulbecco's Modified Eagle Medium (DMEM) (Sigma-Aldrich, D6429) supplemented with 10% heat-inactivated fetal bovine serum (FBS) (Gibco) at 37 ˚C, 5% CO_2. CHO-K1 and CHO cells (kind gifts from Dr. Helena Vihinen and Prof. Mart Saarma, respectively, University of Helsinki) were maintained in the same medium supplemented with 1x non-essential amino acids (NEAA) solution (Lonza). On the day of transfection, conditioned medium was replaced with fresh DMEM medium with 4% FBS and antibiotic-antimycotic mixture (Gibco). NEAA solution was added to the medium when CHO-K1 and CHO cells were used.

HumanRET plasimds were mixed with polyethylenimine (PEI) (Polysciences Europe GmbH) [36] in a 1:3 molar ratio at room temperature (RT) in DMEM medium, the ratio of which was optimized for RET expression (**Supplementary Fig. 1A**), without FBS or antibiotics for 8 min prior to transfection. For the expression of Fc-GDF15, conditioned medium was replaced with DMEM medium containing 1x lipid mixture solution (PeproTech) and 1x serum replacement solution (PeproTech) with antibiotic-antimycotic mixture. Fc-GDF15 and Fc plasmids were mixed at a 2:1 ratio for co-expression and the mixed plasmids were then incubated with PEI in a 1:2.5 molar ratio at RT for 8 min before transfection.

Spodoptera frugiperda (*Sf* 9) and *Trichoplusia ni* High Five (Hi5) cells (Thermo Fisher Scientific) were cultured in suspension at 27 ˚C in Xpress medium (Lonza). Bacmid DNAs containing RET^{ECD} and GFRAL genes were generated and transfection and baculovirus generation was performed as previously described [37]. Baculovirus-infected insect cells (BIIC) were prepared and used for large-scale expression [37].

2.2.1 *Expression optimization*

After the addition of PEI/DNA mixture, cells were incubated at 37 ˚C for 24 h and expression tests were run at either that temperature or at 33 ˚C after the initial incubation at 37 ˚C. Supernatant (SN) samples were taken daily from 4 to 7 days after transfection for HEK293T cells and from 4 to 11 days after transfection for CHO-K1 cells. On Day 7 post-transfection HEK293T cells started to look unhealthy; therefore, we stopped collecting samples for assessing expression.

2.2.2 Large-scale expression

For large-scale expression of RET^{ECD} and Fc-GDF15, adherent HEK293T cells were cultured in either roller bottles (Greiner Bio-One GmbH) at 2 rpm, or 5-layerred flasks (Falcon™, Fisher Scientific) at 37 ˚C, 5% CO2. After transfection, the expression of RET^{ECD} and Fc-GDF15 continued for 7 and 5 days, respectively. For expressing RET^{ECD} in insect cells, *Sf* 9 cells were infected at a cell density of 1 million cells/ml with one vial of BIIC ($1x10^7$ infected cells) per liter culture. GFRAL was expressed using Hi5 cells at the same density with two vials of BIIC ($2x10^7$ infected cells) per liter culture. The amount of BIIC to use for large-scale expression was optimized for each construct so that proliferation arrest was achieved 24-h post-transfection. The expression of RET^{ECD} and GFRAL was then carried out for 72 h and 68 h, respectively.

2.3 Protein purification

Cell culture medium containing the secreted proteins was harvested after the indicated expression time by centrifuging at 4000 rpm for 15 min at 4 ˚C to pellet the cells. For volumes larger than 1 litre, the cleared supernatant was concentrated and buffer-exchanged using a Pellicon concentrator (Millipore EMD). Membranes with a molecular weight (MW) cut off of 10 kDa were used for Fc-GDF15 and GFRAL and with a cut off of 30 kDa for RET^{ECD}. RET^{ECD} expressed using insect and mammalian cells was first immobilized on Ni-NTA resin (Qiagen) and the bound protein was eluted with buffer containing 125 mM imidazole. The elutae was further purified using anti-Flag (GenScript) affinity chromatography and 300 μg/ml poly-Flag peptide (Bimake) was used for protein elution from anti-Flag resin. Purified RET^{ECD} was concentrated with Amicon centrifuge concentrators (30 kDa) and buffer-exchanged into 20 mM HEPES pH 7.5, 150 mM NaCl, 1 mM $CaCl_2$ with 10% glycerol. RET^{C634R*}-Fc was purified as for RET^{ECD} if the Fc tag was not to be cleaved. After peptide elution, RET^{C634R*}-Fc was buffer exchanged and concentrated with Amicon centrifuge concentrators (50 kDa).

To purify the extracellular domain of RET^{C634R*} dimer, medium containing RET^{ECD}-Fc was incubated with pre-equilibrated Protein A resin (GenScript) in binding buffer containing 20 mM HEPES pH 7.5, 150 mM NaCl, 1 mM $CaCl_2$. After washing, His-tagged TEV protease was added to the resin at a molar ratio of 1:10 and the mixture was incubated overnight at 4 ˚C. The cleaved product was loaded onto a HisTrap column (GE Healthcare) to remove impurities, including HIS tags, un-cleaved products and TEV protease and cleaved RET^{C634R*} was eluted at a low imidazole concentration by gradient elution. The fractions containing RET^{C634R*} were concentrated with Amicon centrifuge concentrators (50 kDa) and then purified using size exclusion chromatography (SEC) on a Superdex 200 increase 5/150 GL column (GE Healthcare) in 20 mM HEPES pH 7.5, 100 mM NaCl, 1 mM $CaCl_2$.

Fc-GDF15 was purified using Protein A resin and eluted using 100 mM sodium citrate, 100mM NaCl, pH 3.1. The eluate was collected drop by drop into 100 μl of neutralization buffer containing 1 M Tris pH 8.8 per ml of eluate and the fractions containing Fc-GDF15 were concentrated and buffer exchanged into Tris-buffered

saline (TBS) pH 7.5. GFRAL was purified using Strep-Tactin resin (IBA Lifesciences) and eluted with elution buffer containing 20 mM HEPES pH 7.2, 150 mM NaCl, 5 mM d-Desthiobiotin (IBA Lifesciences). Elution fractions were collected, concentrated and further purified either using SEC on a Hiload Superdex 200 pg 16/600 (GE Healthcare) or a Superdex 200 increase 10/300 column (GE Healthcare) in 20 mM HEPES pH 7.2, 150 mM NaCl.

2.4 Pull-down assays

2.4.1 Activity assessment of insect cell- and mammalian cell-expressed RET^{ECD}

Fc-GDF15 dimer and GFRAL were first incubated together on ice for 15 min. RET^{ECD} expressed using either *Sf* 9 or HEK293T cells was then added to the mixture. The final molar ratio of Fc-GDF15 dimer:GFRAL:RET in the mixture was 1:2:2 (1.25:2.5:2.5 μM). After incubating the samples on ice for 1 h, 5 μl of pre-equilibrated protein A resin in binding buffer containing 20 mM HEPES pH 7.5, 150 mM NaCl, 2 mM $CaCl_2$, 5% glycerol and 0.05% Tween-20 was added to each sample to immobilize Fc-GDF15 via the Fc to pull down either GFRAL or GFRAL and RET^{ECD}. To assess the level of non-specific binding, the same amount of resin was added to samples that only contained RET^{ECD}. Binding buffer was added to each sample to make a final volume of 400 μl and the samples were incubated at 4 ˚C for 1 h with end-to-end rotation. After incubation, the resin was pelleted by centrifuging at 700 x *g* for 2 min at 4 ˚C and washed three times with 500 μl binding buffer. Finally, 15 μl of binding buffer was added to each sample with SDS polyacrylamide gel electrophoresis (SDS-PAGE) sample loading buffer without Dithiothreitol (DTT) to release any bound proteins on the resin for SDS-PAGE and western blotting (WB) analysis with anti-HIS antibody (Qiagen) and anti-mouse-horseradish peroxidase (HRP) secondary antibody (m-IgGκ BP-HRP, Santa Cruz Biotechnology).

2.4.2 Analysis of the expression of RET$^{C634R(*)}$ dimer

HEK293T cells were plated in 12-well tissue culture plates one day before transfection and PEI transfection was carried out as described above at 70% cell confluency. As a negative control, PEI without any plasmid was added to the cells. Supernatant containing the expressed proteins (RET$^{C634R(*)}$-(G_4S)-Fc and RET^{C630A,C634R}-Fc) as well as the control sample was collected 7 days post transfection and centrifuged at high

speed to remove cell debris. Pre-washed protein A resin (10 µl) was directly added to the clarified media. Incubation and washes were performed as described above. After the washing step, 250 µl binding buffer was added to each sample and 60 µl of the resuspended mixture with beads was collected for SDS-PAGE to analyse the expression of the Fc-tagged proteins. His-tagged TEV protease (20 µg) was added to each sample and incubated at 4 ˚C overnight without agitation. The next day, another 60 µl of the resuspended sample was collected to examine total proteins in each sample as well as the cleavage efficiency of TEV protease. The rest of the sample was centrifuged to remove the remaining resin and the supernatant was taken for further analysis. Samples collected before and after the addition of the protease were mixed with SDS-PAGE loading buffer with or without DTT to evaluate the disulfide-bonded $RET^{C634R(*)}$-(GS)-Fc and $RET^{C634R(*)}$ homodimers. The proteins were resolved on 4–20% gradient gels (Bio-Rad), which were subsequently analysed by western blot with anti-RET(C3)-HRP antibody (Santa Cruz Biotechnology).

2.5 Blue native PAGE to visualize complex formation

For the formation of the RET^{ECD}/Fc-GDF15/GFRAL complex, Fc-GDF15 dimer was incubated with GFRAL for 15 min prior to the addition of RET^{ECD}. The final volume was 10 µl, and the final concentrations of Fc-GDF15 dimer, GFRAL and RET^{ECD} are 1.75 µM, 3.5 µM and 3.5 µM, respectively. Fc-GDF15/GFRAL was prepared in the same way without the addition of RET^{ECD}. The protein mixtures were incubated at 4 ˚C for 1 h before the addition of the blue native (BN) PAGE sample buffer. Electrophoresis was carried out using 4–20% gradient gels and run at 100 V for 3.5 h at 4 ˚C as previously described [37,38]. Gels were destained using destaining solution containing 20% methanol and 10% acetic acid and the solution was changed every 20 min until the protein bands were clear against the background.

2.6 Bio-layer interferometry technology system (BLItz)

Anti-hIgG Fc capture (AHC) biosensors (FortéBio) were pre-hydrated in buffer containing 20 mM HEPES pH 7.5, 150 mM NaCl, 1 mM $CaCl_2$ with 0.05% Tween-20 for at least 10 min. Measurements were taken using a BLItz instrument (FortéBio) in 7 steps: initial baseline (30 s), loading (120 s), baseline (60 s), association 1 (180 s), baseline (60 s), association 2 (180 s) and dissociation (180 s). Fc-GDF15 was immobilized to AHC

sensor tips at a concentration of 15 μM in the loading step and GFRAL at a concentration of 3 μM was used to saturate the immobilized Fc-GDF15 in the first association step. A concentration series of 0.11, 0.56, 1.2, 2.8, 7, 14 and 28 μM of RET^{ECD} (mammalian) and a concentration series of 1.2, 2.8, 7, 14 and 28 μM of RET^{ECD} (insect) were used in the second association step to bind to the pre-formed Fc-GDF15/GFRAL complexes. Experiments were performed in triplicate for RET^{ECD} (mammalian) and in duplicate for RET^{ECD} (insect) independently. The sensorgrams of the association of RET^{ECD} as well as the saturation binding curves were plotted with GraphPad Prism 8. The concentration of RET^{ECD} was transformed to logarithmic scale and fitted using a nonlinear regression sigmoidal model to calculate the dissociation constant (K_d).

3. Results

3.1 The impact of expression host on the activity of the extracellular domain of RET receptor tyrosine kinase

To establish the optimum expression system for RET^{ECD}, we evaluated three mammalian (HEK293T, CHO-K1 and CHO) and two insect (*Sf* 9 and Hi5) cell expression systems.

3.1.1 RET^{ECD} expression using mammalian cells

We evaluated a range of purification tags (His_8 (H) and His_8-Flag (HF)) tags and secretion signal peptides for RET^{ECD} expression in HEK293T cells using transient expression. The expression yield proved to be critically dependent on the signal peptide, with the native signaling peptide giving the highest expression yield (**Table 2**). The construct RET^{ECD}-HF with the native peptide was thus chosen for expression optimization and the expression product using this construct is referred to as RET^{ECD} (mammalian) from here onwards.

Expression tests of RET^{ECD} in CHO-K1 and CHO cells showed that CHO cells expressed less RET^{ECD} than CHO-K1 cells under same expression conditions (**Supplementary Fig. 1B**); thus, the expression optimization of RET^{ECD} was carried out using HEK293T and CHO-K1 cell lines (**Fig. 2**). CHO-K1 cells expressed more RET^{ECD} when incubated at 33 ˚C rather than 37 ˚C, while HEK293T cells showed the opposite temperature dependency for RET^{ECD} expression. The highest expression level was achieved 7 days after transfection at 37 ˚C using HEK293T cells and there is no apparent difference in the ligand-binding capacity of RET^{ECD} expressed using HEK393T and CHO-K1 cells (**Supplementary Fig. 2**). In our laboratory, the yield of purified RET^{ECD} is 0.8 – 1 mg per liter of HEK293T culture.

3.1.2 RET^{ECD} expression using insect cells

To express RET^{ECD} using insect cells, we used the baculovirus expression vector system (BEVS). Because insect cells use different secretion signal peptides than mammalian cells, we did not use the native peptide of RET but the signal peptide from ecdysteroid UDP-glucosyltransferase [35]. Maximum expression of RET^{ECD} was observed 72 hours post infection. The yield of purified RET^{ECD} is around 1 mg per liter of *Sf* 9 cell culture.

When expressed using Hi5 cells, almost all RET^{ECD} was seen in the cells instead of being secreted into the medium (data not shown), and so these cells were not used for further studies. RET^{ECD} expressed using *Sf* 9 cells is referred to as RET^{ECD} (insect).

3.1.3 Comparison of purified RET^{ECD} expressed using insect and mammalian cells

RET^{ECD} undergoes extensive post-translation glycosylation and has 12 predicted glycosylation sites, although the functional significance of these is not well understood. Based on their electrophoretic migration on SDS-PAGE under reducing conditions, we observed RET^{ECD} (mammalian) and RET^{ECD} (insect) to have molecular weights of 120 kDa and 95 kDa respectively (**Fig. 3A**) *versus* a calculated peptide mass for this construct of 71 kDa. These differences in apparent MW are due to varying degrees of post-translational glycosylation, presumably as a result of the different glycosylation machinery in mammalian and insect cell systems [39,40]. As shown in **Fig. 3**, RET^{ECD} (insect) showed a higher level of heterogeneity under non-reducing conditions, consisting of monomer, dimer and larger oligomers and the oligomers are presumably linked by disulfide bonds as they were reduced to monomer after the addition of DTT (**Fig. 3A**). Two extra bands below the full-length RET^{ECD} (insect) were observed, which is possibly due to degradation at the C-terminus of RET^{ECD} (insect) because the proteins were reactive towards anti-RET (C-3) antibody (right panel, **Fig. 3A**) and were sensitive to PNGase treatment similarly to full-length RET^{ECD} (insect) (**Supplementary Fig. 3**). In comparison, RET^{ECD} (mammalian) mainly existed as monomer under both reducing and non-reducing conditions in SDS-PAGE. Separated under their native conditions in BN PAGE, higher order oligomeric RET^{ECD} (insect) bands were observed, while RET^{ECD} (mammalian) exits mainly as monomers, consistent with the results of SDS-PAGE (**Fig. 3B**). In addition, further characterization by SEC showed a single peak for RET^{ECD} (mammalian), suggesting a homogenous protein sample, while a large proportion of RET^{ECD} (insect) eluted earlier than RET^{ECD} (mammalian). The results further confirmed the differences in the oligomeric states between RET^{ECD} (mammalian) and RET^{ECD} (insect).

3.1.4 Difference in activity of RET^{ECD} expressed using insect and mammalian cells

To assess the activity of RET^{ECD} (mammalian) and RET^{ECD} (insect), we first used pull-down assays to see whether they could form a complex with GDF15/GFRAL. RET^{ECD} (mammalian) was clearly pulled down by GDF15/GFRAL (**Fig. 4A)**. The signal strength for pull down of RET^{ECD} (insect) was only slightly stronger than that of the bead control, indicating that only a low percentage (2%) of RET^{ECD} (insect) is active. To calculate the relative activity of RET^{ECD} (mammalian) and RET^{ECD} (insect) in binding to GDF15/GFRAL, we compared the intensity of the RET^{ECD} bands for both input and pull-down samples. RET^{ECD} (mammalian) is over 25 times more active than RET^{ECD} (insect) (**Fig. 4B)**.

Additionally, BN PAGE was used to detect RET/GDF15/GFRAL complex formation. As expected, GDF15/GFRAL complex formation as well as its complex with RET^{ECD} (mammalian) (marked by the red star, **Fig. 5**) were observed, confirming their binding capacity. However, no complex formation was seen when RET^{ECD} (insect) was together with GDF15/GFRAL, and the band intensity of monomer and dimer RET^{ECD} (insect) did not change upon the addition of the ligands.

To orthogonally and quantitatively validate these results, we used BLItz to measure the binding affinity between RET^{ECD} and GDF15/GFRAL. Accordingly, Fc-GDF15/GFRAL was immobilized on anti-hIgG Fc biosensors and the concentration dependent binding of both RET^{ECD} (mammalian) and RET^{ECD} (insect) was measured (**Fig. 6A**). In accordance with our previous results, no binding was observed for RET^{ECD} (insect) even at the highest concentration (28 μM) (**Fig. 6B**). Conversely, we observed a concentration dependent association signal for RET^{ECD} (mammalian), giving a calculated K_d of 3.2 μM (2.0 – 5.2 μM, 95% confidence interval) for binding to Fc-GDF15/GFRAL (**Fig. 6C and 6D**).

3.2 Recombinant expression of oncogenic mutant RET^{C634R}

The oncogenic C634R mutation of RET is one of the most common driver mutations associated with MEN 2A and, in the context of full-length RET, is known to drive ligand-independent dimerization of RET. However, previous studies have found that the extracellular domain carrying the C634R mutation does not dimerize when recombinantly expressed, bringing the mechanism of action into question. We sought to use our optimized expression system to interrogate the questions posed by these findings. Therefore, we introduced

the C634R mutation into our optimized expression construct for the ECD of RET and tested the expression in HEK293T cells. Consistent with the previous reports [15,20], we found that the ECD of RET^{C634R} expressed well but existed solely as a monomer, demonstrating that C630 had not formed an intermolecular disulfide bond. We hypothesized that alternative C630 oxidation processes (*eg* to sulfinic acid or sulfonate [41]) might be occurring faster than disulfide-induced dimerization of RET^{C634R} because of the low RET concentration when recombinantly expressed into the oxidizing extracellular medium (**Fig. 7**, upper panel). Therefore, we incorporated a C-terminal Fc tag into the construct to mimic the higher local RET concentrations found in the membrane for full-length oncogenic RET as we expected that intermolecular C630-C630 disulfide formation would then occur (**Fig. 7**, lower panel). Following expression and purification of RET^{C634R}-Fc, SDS-PAGE analysis revealed that RET^{C634R}-Fc exists in dimeric form (MW ~ 300 kDa under non-reducing conditions) and becomes monomeric under reducing conditions (MW ~ 150 kDa) (**Fig. 8**). Following cleavage of the Fc tag by TEV protease, RET^{C634R} remained mainly dimeric (MW ~ 240 kDa under non-reducing conditions) indicating that the Fc tag had induced the expected RET homodimerization and the dimer was not held together only by the Fc. Upon treatment with reducing agent, RET^{C634R} was resolved entirely as a monomer (MW ~ 120 kDa) (**Fig. 8**), demonstrating that the mechanism of homodimerization is *via* disulfide bond formation, supporting our hypothesis. To verify that the disulfide bond formation is through C630, we expressed and purified $RET^{C630A,C634R}$-Fc. This construct expressed well but, after cleavage of Fc tag, was entirely monomeric (Supplementary **Fig. 4**). That the additional C630A mutation abolishes the propensity for RET to dimerize provides further support that the mechanism of C634R dimerization is through intermolecular C630-C630 disulfide bond formation.

Apart from C630, RET^{C634R} contains two additional cysteine residues, C87 and C216, which are known to be unpaired and surface exposed in wild type RET. To eliminate the possibility that C87 or C216 might be the source of intermolecular disulfide induced RET dimerization, we generated a mutant construct, $RET^{C87R, C216S, C634R}$ (RET^{C634R*}-Fc), for which C630 is the only unpaired cysteine (**Table 1**). Similar to RET^{C634R}, the RET^{C634R*} mutant remained dimeric after the Fc tag removal, confirming the hypothesis that it is only the C630-C630 disulfide bond that causes dimerization (**Fig. 8**). Moreover, RET^{C634R*}-Fc showed improved

expression compared to RET^{C634R}-Fc, which is consistent with previous reports where the C87R and C216S mutations have been introduced to wild-type RET^{ECD} [31].

To improve the protein yield further, we generated two additional constructs containing a G_4S linker between the cleavage site and the Fc tag but found that this had no significant impact on either expression level or the efficiency of TEV protease cleavage (**Fig. 8**). Because the RET^{C634R*}-Fc gave higher expression than RET^{C634R}-Fc, we scaled up expression of RET^{C634R*}-Fc in HEK293T cells without the G_4S linker for further characterization. Following our expression and two-step purification protocol, we obtained RET^{C634R*}-Fc dimer with a yield of 2.9 mg per liter of culture and a purity higher than 90%, calculated based on the band intensity of the Coomassie-stained SDS-PAGE (**Fig. 9A**). For the purification of RET^{C634R*}, following TEV protease cleavage, the dimer was co-purified with a 25% contamination of RET^{C634R*} monomer. These could be separated by SEC (**Fig. 9B**) and the final yield of RET^{C634R*} dimer was 400 μg per liter of culture.

4. Discussion

Both insect and mammalian cell expression systems have been used for recombinant protein expression of either the extracellular domains or full-length RTKs. So far, only mammalian cells have been reported to express RET^{ECD}; we therefore compared the expression of RET^{ECD} in insect cells to its expression in mammalian cells. The expression levels of RET^{ECD} in both systems were comparable, yielding 0.8-1 mg per liter culture. However, only RET^{ECD} (mammalian), not RET^{ECD} (insect), can bind to its ligands (**Fig. 3** and **Fig. 4**). Glycosylation is known to be important for the proper folding of RET and other RTKs [20,32,42,43]. We observed that both RET^{ECD} (mammalian) and RET^{ECD} (insect) were heavily glycosylated, with RET^{ECD} (mammalian) carrying approximately 51 kDa of glycosylation and RET^{ECD} (insect) approximately 24 kDa (**Fig. 3A**). The difference in the glycosylation level was expected as mammalian cells produce more complex glycan chains in their N-glycan processing pathway than insect cells [44]. One way to assess whether glycoproteins have been properly post-translationally processed is to measure their sensitivity to PNGase and Endo H [45,46]: In the Golgi, complex N-glycans are added to the glycoproteins, rendering them Endo H-resistant [47]. In our study, RET^{ECD} (insect) was secreted by *Sf* 9 insect cells and the purified protein was sensitive to PNGase but not Endo H_f (**Supplementary Fig. 3**), indicating that the protein was processed through the ER and Golgi. However, RET^{ECD} expressed in Hi5 cells could not be secreted, suggesting substantial misfolding of RET^{ECD} in Hi5 cells and indicating that different insect cell lines express complex mammalian proteins differently.

HumanRET^{ECD} contains 28 cysteine residues. Apart from two unpaired cysteines, C87 and C216, the others form 13 intramolecular disulfide bonds, which gives rise to the risk of disulfide mismatching during post-translation processing. The CLDs 1-3 of humanRET have also been reported to be more prone to misfold when compared to the non-mammal species [20]. In our study, RET^{ECD} expressed using *Sf* 9 cells exhibited various higher order oligomeric states cross-linked by disulfide bonds (**Fig. 3**). While RET^{ECD} (mammalian) could form a complex with GDF15/GFRAL with a K_d of 3.2 μM, little or no apparent complex formation was seen between RET^{ECD} (insect) and GDF15/GFRAL (**Figs. 4-6**). To our knowledge, this is the first time the affinity between humanRET^{ECD} and GDF15/GFRAL has been quantitatively reported. Although different to that reported for humanRET^{ECD} binding to GDNF/GFRα1-Fc (15 nM) measured by enzyme-linked

immunosorbent assay (ELISA) [31], the measured affinity is similar to that reported for zebrafishRET^{ECD} binding to GDNF/GFRα1 (5.9 μM) measured, as we did, by BLItz [48]. Such conservation of affinity is expected as a result of the conserved activation mechanism among GFLs and GDF15 signalling through RET [9,16] and is further demonstration that our proteins are fully active. Overall, the results suggest that insect cells do not express functional humanRET^{ECD}, likely due to disulfide-mismatch-induced misfolding. This may explain why, when expressed in Hi5 cells, humanRET^{ECD} could not be secreted [49], even though we previously showed that Hi5 cells could express functional, monomeric zebrafishRET^{ECD}, which contains fewer cysteine residues compared to humanRET^{ECD} [37].

Different approaches have been reported for the expression of recombinant humanRET^{ECD} using mammalian cells (**Supplementary Table 1**). In our study, we compared transient expression of RET^{ECD} in HEK293T, CHO-K1 and CHO cells. We found that HEK293T cells showed highest expression, CHO-K1 cells second, and CHO cells expressed most poorly (**Fig. 2** and **Supplementary Fig. 1**). In accordance with previous results [20], the expression of RET^{ECD} is better at lower temperature using CHO-K1 cells, but we observed high expression of RET^{ECD} using HEK293T cells only at 37 °C (**Fig. 2**). It is likely that the higher expression level results from a balance between the high cellular activity of HEK cells at 37 ˚C and rate-limiting misfolding potential. Furthermore, we used HEK293T cells to express some of the RET^{ECD} glycosylation mutants (N336Q, N343Q and N468Q) (**Table 1**). We found that the expression level of RET^{N336Q} was similar to that of wild-type RET^{ECD} (0.8-1 mg per liter culture) while that of two other mutants, N343Q and N468Q, was three times lower (0.3 mg per liter culture) (**Supplementary Fig. 5A**). Based on the result from pull-down assays, the binding capacity of the purified mutants (N336Q and N343Q) to GDF15/GFRAL is comparable to that of the wild-type RET^{ECD} (**Supplementary Fig. 5B and 5C**). It would be interesting to further investigate whether these or other glycosylation mutants significantly impact RET stability and function.

RET dimerization of the oncogenic C634R mutant is one of the most common mechanisms causing MEN 2A. Here we demonstrated that, by attaching a C-terminal Fc tag to RET^{C634R}, the extracellular domain of the oncogenic mutant could be expressed and purified in its dimeric form. Previous attempts showed that the recombinantly expressed ECD of soluble RET ^{C634R} showed no apparent difference to that of wild type RET

[15,20], but dimerization of full-length RET^{C634R} has been reported to occur readily [50–53]. We hypothesized that the dimerization of full-length mutant RET via cysteine residue C630 occurs due to the high effective concentration of RET in the membrane and the fact that all of the protein is correctly oriented to place the two C630s near each other. Conversely, in soluble RET^{ECD} expressed recombinantly, C630 will be oxidized *eg* to sulfinic acid and sulfonates [41] at the low protein concentrations present in the extracellular medium, thus disfavoring RET-RET dimerization (**Fig. 7**). Therefore, the addition of the Fc tag to the C-terminus of RET, bringing the C-terminus of two RET^{ECD}s close to each other, would enable the dimer formation of soluble RET^{C634R}. Our results were consistent with this: we obtained 75% of dimeric RET^{C634R*} after tag removal (**Fig. 9**). There are two explanations for why 25% remained monomeric. One possibility is that this is an artefact introduced by the reducing reagent (50 μM TCEP) that is necessary for efficient proteolytic tag removal by TEV protease; the other is that there is only 75% formation of the C630 crosslink. This could be tested by using cysteine-independent proteases for tag removal, such as Thrombin, to enable cleavage of the Fc tag under non-reducing conditions.

Our studies of RET^{ECD} expressed using insect and mammalian cells showed the impact of the eukaryotic expression hosts on protein function and emphasize that caution should be taken when using insect cell expression systems especially for cysteine-rich and highly glycosylated proteins that are prone to misfold. Successful purification of soluble dimeric RET^{C634R} provides a route for further functional and structural studies to understand oncogenic activation of RET and its role in driving cancers such as MEN 2A.

5. Acknowledgements

We thank Dr. Bernadette Gehl (University of Helsinki, Finland) for kindly helping with insect and mammalian cell culture and DNA preparations, Dr. Euan Baxter (University of Leeds, UK) for his help with mammalian cell culture, Mr. Tuukka Eerikkilä for his support in the laboratory (University of Helsinki, Finland) and Dr. Gregory Craven (University of Leeds, UK) for his help in revising the manuscript. We thank Dr. Hideo Iwai (University of Helsinki, Finland) and the facilities and expertise of the HiLIFE NMR unit at the University of Helsinki, a member of Instruct-ERIC Centre Finland, FINStruct, and Biocenter Finland, for the access to the bio-layer interferometry instrument.

6. References

[1] L.M. Mulligan, GDNF and the RET receptor in cancer: New insights and therapeutic potential, *Front. Physiol.* 10 (2019). https://doi.org/10.3389/fphys.2018.01873.

[2] T. Kohno, J. Tabata, T. Nakaoku, REToma: a cancer subtype with a shared driver oncogene, *Carcinogenesis*. (2019). https://doi.org/10.1093/carcin/bgz184.

[3] C.F. Ibáñez, Structure and physiology of the RET receptor tyrosine kinase, *Cold Spring Harb. Perspect. Biol.* 5 (2013) a009134–a009134. https://doi.org/10.1101/cshperspect.a009134.

[4] P.T. Kotzbauer, P.A. Lampe, R.O. Heuckeroth, J.P. Golden, D.J. Creedon, E.M. Johnson Jr, J. Milbrandt, Neurturin, a relative of glial-cell-line-derived neurotrophic factor, *Nature.* 384 (1996) 467–470. https://doi.org/10.1038/384467a0.

[5] J. Milbrandt, F.J. De Sauvage, T.J. Fahrner, R.H. Baloh, M.L. Leitner, M.G. Tansey, P.A. Lampe, R.O. Heuckeroth, P.T. Kotzbauer, K.S. Simburger, J.P. Golden, J.A. Davies, R. Vejsada, A.C. Kato, M. Hynes, D. Sherman, M. Nishimura, L.C. Wang, R. Vandlen, B. Moffat, R.D. Klein, K. Poulsen, C. Gray, A. Garces, C.E. Henderson, H.S. Phillips, E.M. Johnson, Persephin, a novel neurotrophic factor related to GDNF and neurturin, *Neuron.* 20 (1998) 245–253. https://doi.org/10.1016/S0896-6273(00)80453-5.

[6] R.H. Baloh, M.G. Tansey, P.A. Lampe, T.J. Fahrner, H. Enomoto, K.S. Simburger, M.L. Leitner, T. Araki, E.M. Johnson, J. Milbrandt, Artemin, a novel member of the GDNF ligand family, supports peripheral and central neurons and signals through the GFRα3-RET receptor complex, *Neuron*. 21 (1998) 1291–1302. https://doi.org/10.1016/S0896-6273(00)80649-2.

[7] M. Trupp, E. Arenas, M. Fainzilber, A.-S. Nilsson, B.-A. Sieber, M. Grigoriou, C. Kilkenny, E. Salazar-Grueso, V. Pachnis, U. Arumäe, H. Sariola, M. Saarma, C.F. Ibáñez, Functional receptor for GDNF encoded by the c-ret proto-oncogene, *Nature*. 381 (1996) 785–789. https://doi.org/10.1038/381785a0.

[8] P. Durbec, C. V. Marcos-Gutierrez, C. Kilkenny, M. Grigoriou, K. Wartiowaara, P. Suvanto, D. Smith, B. Ponder, F. Costantini, M. Saarma, H. Sariola, V. Pachnis, GDNF signalling through the Ret receptor tyrosine kinase, *Nature.* 381 (1996) 789–793. https://doi.org/10.1038/381789a0.

[9] J.-Y. Hsu, S. Crawley, M. Chen, D.A. Ayupova, D.A. Lindhout, J. Higbee, A. Kutach, W. Joo, Z. Gao, D. Fu, C. To, K. Mondal, B. Li, A. Kekatpure, M. Wang, T. Laird, G. Horner, J. Chan, M. McEntee, M. Lopez, D. Lakshminarasimhan, A. White, S.-P. Wang, J. Yao, J. Yie, H. Matern, M. Solloway, R. Haldankar, T. Parsons, J. Tang, W.D. Shen, Y. Alice Chen, H. Tian, B.B. Allan, Non-homeostatic body weight regulation through a brainstem-restricted receptor for GDF15, *Nature.* 550 (2017) 255–259. https://doi.org/10.1038/nature24042.

[10] S.E. Mullican, X. Lin-Schmidt, C.-N. Chin, J.A. Chavez, J.L. Furman, A.A. Armstrong, S.C. Beck, V.J. South, T.Q. Dinh, T.D. Cash-Mason, C.R. Cavanaugh, S. Nelson, C. Huang, M.J. Hunter, S.M. Rangwala, GFRAL is the receptor for GDF15 and the ligand promotes weight loss in mice and nonhuman primates, *Nat. Med.* 23 (2017) 1150–1157. https://doi.org/10.1038/nm.4392.

[11] L. Yang, C.-C. Chang, Z. Sun, D. Madsen, H. Zhu, S.B. Padkjær, X. Wu, T. Huang, K. Hultman, S.J. Paulsen, J. Wang, A. Bugge, J.B. Frantzen, P. Nørgaard, J.F. Jeppesen, Z. Yang, A. Secher, H. Chen, X. Li, L.M. John, B. Shan, Z. He, X. Gao, J. Su, K.T. Hansen, W. Yang, S.B. Jørgensen, GFRAL is the receptor for GDF15 and is required for the anti-obesity effects of the ligand, *Nat. Med.* 23 (2017) 1158–1166. https://doi.org/10.1038/nm.4394.

[12] P.J. Emmerson, F. Wang, Y. Du, Q. Liu, R.T. Pickard, M.D. Gonciarz, T. Coskun, M.J. Hamang, D.K. Sindelar, K.K. Ballman, L.A. Foltz, A. Muppidi, J. Alsina-Fernandez, G.C. Barnard, J.X. Tang, X. Liu, X. Mao, R. Siegel, J.H. Sloan, P.J. Mitchell, B.B. Zhang, R.E. Gimeno, B. Shan, X. Wu, The metabolic effects of GDF15 are mediated by the orphan receptor GFRAL, *Nat. Med.* 23 (2017) 1215–1219. https://doi.org/10.1038/nm.4393.

[13] D.H.J. Van Weering, T.C. Moen, I. Braakman, P.D. Baas, J.L. Bos, Expression of the receptor tyrosine kinase Ret on the plasma membrane is dependent on calcium, *J. Biol. Chem.* 273 (1998) 12077–12081. https://doi.org/10.1074/jbc.273.20.12077.

[14] J. Anders, S. Kjær, C.F. Ibáñez, Molecular modeling of the extracellular domain of the RET receptor tyrosine kinase reveals multiple cadherin-like domains and a calcium-binding site, *J. Biol. Chem.* 276 (2001) 35808–35817. https://doi.org/10.1074/jbc.M104968200.

[15] K.M. Goodman, S. Kjær, F. Beuron, P.P. Knowles, A. Nawrotek, E.M. Burns, A.G. Purkiss, R.

George, M. Santoro, E.P. Morris, N.Q. McDonald, RET recognition of GDNF-GFRα1 ligand by a composite binding site promotes membrane-proximal self-association, *Cell Rep.* 8 (2014) 1894–1904. https://doi.org/10.1016/j.celrep.2014.08.040.

[16] J. Li, G. Shang, Y.-J. Chen, C.A. Brautigam, J. Liou, X. Zhang, X. Bai, Cryo-EM analyses reveal the common mechanism and diversification in the activation of RET by different ligands, *Elife*. 8 (2019). https://doi.org/10.7554/eLife.47650.

[17] J.M. Bigalke, S. Aibara, R. Roth, G. Dahl, E. Gordon, S. Dorbéus, A. Amunts, J. Sandmark, Cryo-EM structure of the activated RET signaling complex reveals the importance of its cysteine-rich domain, *Sci. Adv.* 5 (2019) eaau4202. https://doi.org/10.1126/sciadv.aau4202.

[18] S. Wagner, S. Zhu, A. Nicolescu, L. Mulligan, Molecular mechanisms of RET receptor-mediated oncogenesis in multiple endocrine neoplasia 2, *Clinics*. 67 (2012) 77–84. https://doi.org/10.6061/clinics/2012(Sup01)14.

[19] C. Romei, R. Ciampi, R. Elisei, A comprehensive overview of the role of the RET proto-oncogene in thyroid carcinoma, *Nat. Rev. Endocrinol.* 12 (2016) 192–202. https://doi.org/10.1038/nrendo.2016.11.

[20] S. Kjær, C.F. Ibáñez, Intrinsic susceptibility to misfolding of a hot-spot for Hirschsprung disease mutations in the ectodomain of RET, *Hum. Mol. Genet.* 12 (2003) 2133–2144. https://doi.org/10.1093/hmg/ddg227.

[21] R. Roskoski, A. Sadeghi-Nejad, Role of RET protein-tyrosine kinase inhibitors in the treatment RET-driven thyroid and lung cancers, *Pharmacol. Res.* 128 (2018) 1–17. https://doi.org/10.1016/j.phrs.2017.12.021.

[22] R. Roskoski, Classification of small molecule protein kinase inhibitors based upon the structures of their drug-enzyme complexes, *Pharmacol. Res.* 103 (2016) 26–48. https://doi.org/10.1016/j.phrs.2015.10.021.

[23] J.L. Gilmore, D.J. Riese, secErbB4-26/549 antagonizes ligand-induced ErbB4 tyrosine phosphorylation, *Oncol. Res.* 14 (2004) 589–602. https://doi.org/10.3727/0965040042707907.

[24] L.Z. Mi, M.J. Grey, N. Nishida, T. Walz, C. Lu, T.A. Springer, Functional and structural stability of the epidermal growth factor receptor in detergent micelles and phospholipid nanodiscs, *Biochemistry*. 47 (2008) 10314–10323. https://doi.org/10.1021/bi801006s.

[25] J.P. Dawson, M.B. Berger, C.-C. Lin, J. Schlessinger, M.A. Lemmon, K.M. Ferguson, Epidermal growth factor receptor dimerization and activation require ligand-induced conformational changes in the dimer interface, *Mol. Cell. Biol.* 25 (2005) 7734–7742. https://doi.org/10.1128/MCB.25.17.7734-7742.2005.

[26] H. Ogiso, R. Ishitani, O. Nureki, S. Fukai, M. Yamanaka, J.H. Kim, K. Saito, A. Sakamoto, M. Inoue, M. Shirouzu, S. Yokoyama, Crystal structure of the complex of human epidermal growth factor and receptor extracellular domains, *Cell*. 110 (2002) 775–787. https://doi.org/10.1016/S0092-8674(02)00963-7.

[27] K. Xu, D. Tzvetkova-Robev, Y. Xu, Y. Goldgur, Y.P. Chan, J.P. Himanen, D.B. Nikolov, Insights into Eph receptor tyrosine kinase activation from crystal structures of the EphA4 ectodomain and its complex with ephrin-A5, *Proc. Natl. Acad. Sci. U. S. A.* 110 (2013) 14634–14639. https://doi.org/10.1073/pnas.1311000110.

[28] S. Paavilainen, D. Grandy, E. Karelehto, E. Chang, P. Susi, H. Erdjument-Bromage, D.B. Nikolov, J.P. Himanen, High-level expression of a full-length Eph receptor, *Protein Expr. Purif.* 92 (2013) 112–118. https://doi.org/10.1016/j.pep.2013.08.016.

[29] J.P. Himanen, L. Yermekbayeva, P.W. Janes, J.R. Walker, K. Xu, L. Atapattu, K.R. Rajashankar, A. Mensinga, M. Lackmann, D.B. Nikolov, S. Dhe-Paganon, Architecture of Eph receptor clusters, *Proc. Natl. Acad. Sci.* 107 (2010) 10860–10865. https://doi.org/10.1073/pnas.1004148107.

[30] L. Ivanisevic, W.H. Zheng, S.B. Woo, K.E. Neet, H.U. Saragovi, TrkA receptor "hot spots" for binding of NT-3 as a heterologous ligand, *J. Biol. Chem.* 282 (2007) 16754–16763. https://doi.org/10.1074/jbc.M701996200.

[31] S. Kjær, S. Hanrahan, N. Totty, N.Q. McDonald, Mammal-restricted elements predispose human RET to folding impairment by HSCR mutations, *Nat. Struct. Mol. Biol.* 17 (2010) 726–731. https://doi.org/10.1038/nsmb.1808.

[32] I.G. Ferreira, M. Pucci, G. Venturi, N. Malagolini, M. Chiricolo, F. Dall'Olio, Glycosylation as a main regulator of growth and death factor receptors signaling, *Int. J. Mol. Sci.* 19 (2018) 580.

https://doi.org/10.3390/ijms19020580.
[33] Y. Xiong, K. Walker, X. Min, C. Hale, T. Tran, R. Komorowski, J. Yang, J. Davda, N. Nuanmanee, D. Kemp, X. Wang, H. Liu, S. Miller, K.J. Lee, Z. Wang, M.M. Véniant, Long-acting MIC-1/GDF15 molecules to treat obesity: Evidence from mice to monkeys, *Sci. Transl. Med.* 9 (2017) eaan8732. https://doi.org/10.1126/scitranslmed.aan8732.
[34] Growth differentiation factor 15 (gdf-15) polypeptides, WO2013113008A1, 2015.
[35] M.L. Laukkanen, C. Oker-Blom, K. Keinänen, Secretion of green fluorescent protein from recombinant baculovirus-infected insect cells, *Biochem. Biophys. Res. Commun.* 226 (1996) 755–761. https://doi.org/10.1006/bbrc.1996.1425.
[36] P.A. Longo, J.M. Kavran, M.-S. Kim, D.J. Leahy, Transient mammalian cell transfection with polyethylenimine (PEI), in: Methods Enzymol., Academic Press Inc., 2013: pp. 227–240. https://doi.org/10.1016/B978-0-12-418687-3.00018-5.
[37] Y. Liu, H. Kaljunen, A. Pavić, T. Saarenpää, J.P. Himanen, D.B. Nikolov, A. Goldman, Binding of EphrinA5 to RET receptor tyrosine kinase: An in vitro study, *PLoS One*. 13 (2018) e0198291. https://doi.org/10.1371/journal.pone.0198291.
[38] I. Wittig, H.-P. Braun, H. Schägger, Blue native PAGE, *Nat. Protoc.* 1 (2006) 418–428. https://doi.org/10.1038/nprot.2006.62.
[39] J.B. Goh, S.K. Ng, Impact of host cell line choice on glycan profile, *Crit. Rev. Biotechnol.* 38 (2018) 851–867. https://doi.org/10.1080/07388551.2017.1416577.
[40] X. Shi, D. Jarvis, Protein N-glycosylation in the baculovirus-insect cell system, *Curr. Drug Targets*. 8 (2007) 1116–1125. https://doi.org/10.2174/138945007782151360.
[41] C.R. Borges, N.D. Sherma, Techniques for the analysis of cysteine sulfhydryls and oxidative protein folding, *Antioxid. Redox Signal.* 21 (2014) 511–531. https://doi.org/10.1089/ars.2013.5559.
[42] S.R. Hanson, E.K. Culyba, T.-L. Hsu, C.-H. Wong, J.W. Kelly, E.T. Powers, The core trisaccharide of an N-linked glycoprotein intrinsically accelerates folding and enhances stability, *Proc. Natl. Acad. Sci.* 106 (2009) 3131–3136. https://doi.org/10.1073/pnas.0810318105.
[43] E. Klaver, P. Zhao, M. May, H. Flanagan-Steet, H.H. Freeze, R. Gilmore, L. Wells, J. Contessa, R. Steet, Selective inhibition of N-linked glycosylation impairs receptor tyrosine kinase processing, *Dis. Model. Mech.* 12 (2019) dmm039602. https://doi.org/10.1242/dmm.039602.
[44] R.L. Harrison, D.L. Jarvis, Protein N-glycosylation in the baculovirus–insect cell expression system and engineering of insect cells to produce "mammalianized" recombinant glycoproteins, in: Adv. Virus Res., Academic Press, 2006: pp. 159–191. https://doi.org/10.1016/S0065-3527(06)68005-6.
[45] A.L. Tarentino, C.M. Gomez, T.H. Plummer, Deglycosylation of asparagine-linked glycans by peptide:N-glycosidase F, *Biochemistry*. 24 (1985) 4665–4671. https://doi.org/10.1021/bi00338a028.
[46] A.L. Tarentino, R.B. Trimble, T.H. Plummer, Chapter 5 Enzymatic approaches for studying the structure, synthesis, and processing of glycoproteins, in: Methods Cell Biol., Academic Press, 1989: pp. 111–139. https://doi.org/10.1016/S0091-679X(08)61169-3.
[47] X. Zhang, Y. Wang, Glycosylation quality control by the Golgi structure, *J. Mol. Biol.* 428 (2016) 3183–3193. https://doi.org/10.1016/j.jmb.2016.02.030.
[48] T. Saarenpää, K. Kogan, Y. Sidorova, A.K. Mahato, I. Tascón, H. Kaljunen, L. Yu, J. Kallijärvi, J. Jurvansuu, M. Saarma, A. Goldman, Zebrafish GDNF and its co-receptor GFRα1 activate the human RET receptor and promote the survival of dopaminergic neurons in vitro, *PLoS One*. 12 (2017) e0176166. https://doi.org/10.1371/journal.pone.0176166.
[49] C.J. Guerriero, J.L. Brodsky, The delicate balance between secreted protein folding and endoplasmic reticulum-associated degradation in human physiology, *Physiol. Rev.* 92 (2012) 537–576. https://doi.org/10.1152/physrev.00027.2011.
[50] D.H. Arlt, B. Baur, B. Wagner, W. Höppner, A novel type of mutation in the cysteine rich domain of the RET receptor causes ligand independent activation, *Oncogene*. 19 (2000) 3445–3448. https://doi.org/10.1038/sj.onc.1203688.
[51] I. Bongarzone, E. Vigano, L. Alberti, P. Mondellini, M. Uggeri, B. Pasini, M.G. Borrello, M.A. Pierotti, The Glu632-Leu633 deletion in cysteine rich domain of Ret induces constitutive dimerization and alters the processing of the receptor protein, *Oncogene*. 18 (1999) 4833–4838. https://doi.org/10.1038/sj.onc.1202848.
[52] S. Chappuis-Flament, A. Pasini, G. De Vita, C. Ségouffin-Cariou, A. Fusco, T. Attié, G.M. Lenoir, M. Santoro, M. Billaud, Dual effect on the RET receptor of MEN 2 mutations affecting specific

extracytoplasmic cysteines, *Oncogene*. 17 (1998) 2851–2861. https://doi.org/10.1038/sj.onc.1202202.
[53] F. Carlomagno, G. Salvatore, A.M. Cirafici, G. De Vita, R.M. Melillo, V. De Francisas, M. Billaud, A. Fusco, M. Santoro, The different RET-activating capability of mutations of cysteine 620 or cysteine 634 correlates with the multiple endocrine neoplasia type 2 disease phenotype, *Cancer Res.* 57 (1997) 391–395.
[54] J. Schindelin, I. Arganda-Carreras, E. Frise, V. Kaynig, M. Longair, T. Pietzsch, S. Preibisch, C. Rueden, S. Saalfeld, B. Schmid, J.-Y. Tinevez, D.J. White, V. Hartenstein, K. Eliceiri, P. Tomancak, A. Cardona, Fiji: an open-source platform for biological-image analysis, *Nat. Methods*. 9 (2012) 676–682. https://doi.org/10.1038/nmeth.2019.

Table 1*. A summary of transfection constructs used in this study.*

Construct	**Cloned residues**	**Signal peptide**	**Vector**	**Referred in this paper**
RET^{ECD}-TEV-H	28-635	Igκ	pcDNA3.1	
RET^{ECD}-TEV-HF	28-635	Igκ	pcDNA3.1	
RET^{ECD}-TEV-HF	28-635	CD33	pcDNA3.1	
RET^{ECD}-TEV-HF	1-635	Native	pcDNA3.1	RET^{ECD} (mammalian)
RET^{ECD}(C634R)-TEV-Fc-HF	1-635	Native	pcDNA3.1	RET^{C634R}-Fc
RET^{ECD}(C634R)-TEV-G_4S-Fc-HF	1-635	Native	pcDNA3.1	
RET^{ECD}(C634R, C87R, C216S)-TEV-Fc-HF	1-635	Native	pcDNA3.1	RET^{C634R*}-Fc
RET^{ECD}(C634R, C87R, C216S)-TEV-G_4S-Fc-HF	1-635	Native	pcDNA3.1	
RET^{ECD}(C630A, C634R)-TEV-Fc-HF	1-635	Native	pcDNA3.1	$RET^{C630A,C634R}$-Fc
RET^{ECD}(N336Q)-TEV-HF	1-635	Native	pcDNA3.1	RET^{N336Q}
RET^{ECD}(N343Q)-TEV-HF	1-635	Native	pcDNA3.1	RET^{N343Q}
RET^{ECD}(N468Q)-TEV-HF	1-635	Native	pcDNA3.1	RET^{N468Q}
Fc-Thrombin-GDF15	195-308	Igκ	pcDNA3.1	Fc-GDF15
Fc	/	Igκ	pIRES-eGFP	
FH-Thrombin-RET^{ECD}	28-635	Ecdysteroid UDP-glucosyltransferase	pK503.9	RET^{ECD} (insect)
$GFRAL^{ECD}$-TEV-HS	19-351	Ecdysteroid UDP-glucosyltransferase	pK503.9	GFRAL

Table 2. *Expression test of RET^{ECD} with different secretion peptides and tags using HEK293T cells. H: His_8 tag; HF: His_8-Flag tag.*

Signal peptide	**Signal peptide sequence**	**Protein of interest**	**Estimated yield (mg) per liter**
Igκ	METDTLLLWVLLLWVPGSTGD	RET^{ECD}-H	0.02
		RET^{ECD}-HF	0.10
CD33	MPLLLLLPLLWAGALAM	RET^{ECD}-HF	0.45
Native	MAKATSGAAGLRLLLLLLLPLLGKVALG	RET^{ECD}-HF	3.00

Figure legends

Figure 1. Schematic representation of RET activation mechanisms. RET is colored blue, GFRAL red and GDF15 yellow. The coils represent transmembrane helices; GFRAL, as RET, has a single transmembrane helix. P represents phosphorylated tyrosine residues after receptor activation.

Figure 2. Time and temperature dependent comparison of the expression level of RET^{ECD} using HEK293T and CHO-K1 cell lines. Protein expression level of RET^{ECD} was calculated based on band intensity reading from ImageJ [54] (**Supplementary Fig. 1C**). Expression level under each condition is normalized against the highest expression value (Day 7, HEK293T 37 ˚C). Because the majority of HEK293T cells were dying 7 days post transfection, samples were not taken afterwards.

Figure 3. Purified RET^{ECD} expressed using insect and mammalian cells. **A**) Coomassie-stained SDS-PAGE image and anti-RET WB showing purified RET^{ECD} (2 μg) under reducing and non-reducing conditions; **B**) BN PAGE using 1 μg and 2 μg of RET^{ECD} showing the oligomeric state of purified RET^{ECD}; **C**) SEC profile showing different RET^{ECD} expressed using insect (blue) and mammalian cells (beige). M(i): monomeric RET^{ECD} (insect); D(i): dimeric RET^{ECD} (insect); O(i): oligomeric RET^{ECD} (insect); M(m): monomeric RET^{ECD} (mammalian); D(m): dimeric RET^{ECD} (mammalian).

Figure 4. Pull-down of RET expressed using insect and mammalian cells by Fc-GDF15/GFRAL using protein A resin showing that both Fc-GDF15 and GFRAL are required to pull down RET, and that they pull down mammalian-expressed RET. **A**) Left panel shows Coomassie-stained SDS-PAGE image. The area shown in dotted lines was subject to anti-HIS WB (right panel). All samples were treated with SDS loading dye without DTT. Under the denaturing conditions, Fc-GDF15 appears as two major bands with the high MW band being dimeric Fc-GDF15 and the low MW band being Fc. M(i): monomeric RET^{ECD} (insect); D(i): dimeric RET^{ECD} (insect); M(m): monomeric RET^{ECD} (mammalian). **B**) The table shows the band intensity measured by ImageJ

(Area (U)). Bands correspond to RET^{ECD} monomers are labelled (1 for RET^{ECD} (insect) and 2 for RET^{ECD} (mammalian)). U: units.

Figure 5. BN PAGE image showing complex formation of RET/GDF15/GFRAL complex with RET^{ECD} (mammalian) but not with RET^{ECD} (insect). The red star marks the band corresponding to the RET/GDF15/GFRAL complex and the black stars mark the bands corresponding to the GDF15/GFRAL complex. The band observed above the complex band may be attributed to a higher order complex. Fc-GDF15 appears as three bands with the major band corresponding to the desired dimeric Fc_2-GDF15 while the minor bands likely arise from partial Fc dissociation during PAGE.

Figure 6. Measurement of the binding of RET^{ECD} for Fc-GDF15/GFRAL using BLItz. **A**) Schematic diagram of the experimental setup using BLItz; **B,C**) Sensorgrams of RET^{ECD} (insect) (**B**) and RET^{ECD} (mammalian) (**C**) binding to Fc-GDF15/GFRAL immobilized on anti-hIgG Fc (AHC) biosensors at the indicated concentrations; **D**) Saturation binding curves fitted with nonlinear regression sigmoidal model after transforming the concentration to logarithmic scale. CI: Confidence interval.

Figure 7. Schematic representation of different approaches to produce the extracellular domain of RET^{C634R}. Upper panel showing the expression of soluble RET^{C634R} with a possibly oxidized [O] C630 residue. Lower panel showing the expression of RET^{C634R}-Fc as well as the purification of the dimeric RET^{C634R} after Fc tag cleavage by TEV protease. S[O] represents the thiol oxidization of the C630 residue.

Figure 8. Anti-RET WB showing the expression of RET^{C634R}-Fc, RET^{C634R*}-Fc, RET^{C634R}-G_4S-Fc and RET^{C634R*}-G_4S-Fc as well as RET^{C634R} and RET^{C634R*} dimer after Fc tag removal. A G_4S linker was introduced between TEV protease cleavage site and Fc tag in the constructs for RET^{C634R}-Fc and RET^{C634R*}-Fc expression to compare TEV protease cleavage efficiency. Samples were prepared under non-reducing (- DTT) and reducing conditions (+ DTT). B: Protein A beads; S: Supernatant sample after spinning down the beads.

Figure 9. Purification of RET^{C634R} and RET^{C634R}-Fc expressed in HEK293T cells. **A**) Coomassie-stained SDS-PAGE image showing purified extracellular domain of RET^{C634R} with an Fc tag and RET^{C634R} dimer under reducing (right panel) and non-reducing conditions (left panel); **B**) SEC profile showing RET^{C634R} dimer and monomer separation using an S200 increase 5/150 column.

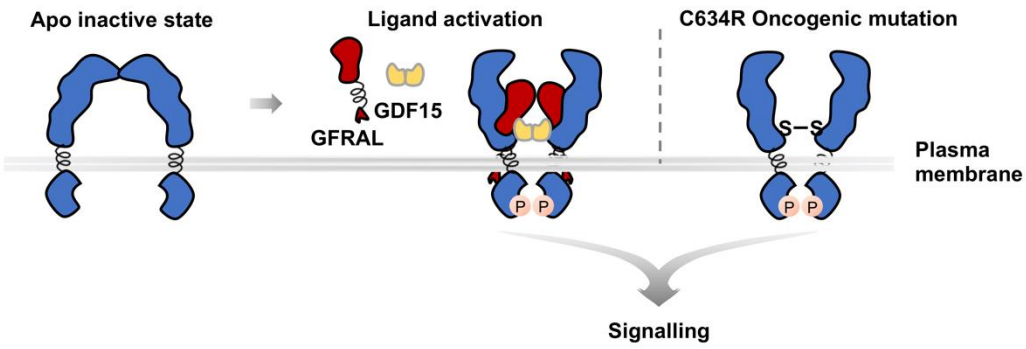

International Journal of Biological Macromolecules, Liu et al. Fig.1

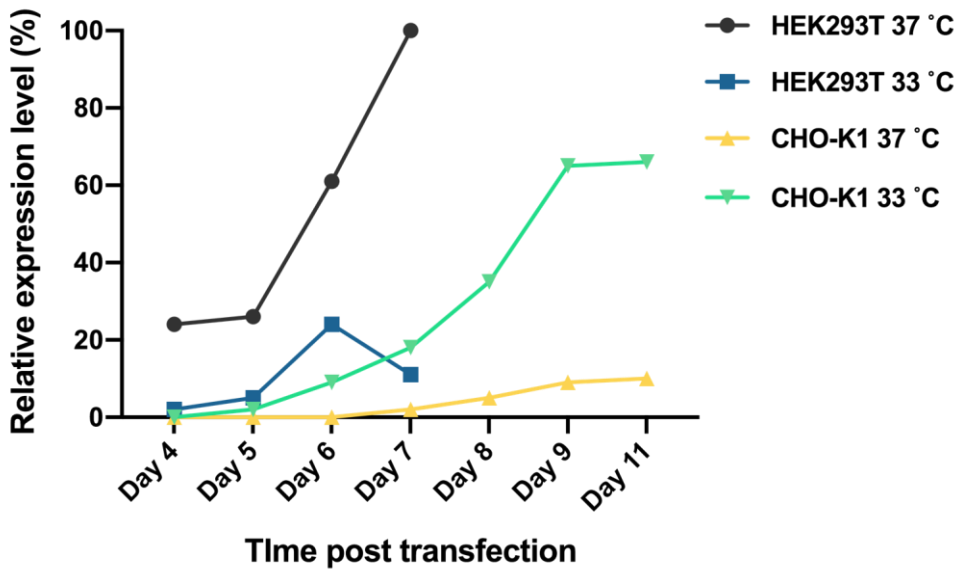

International Journal of Biological Macromolecules, Liu et al. Fig.2

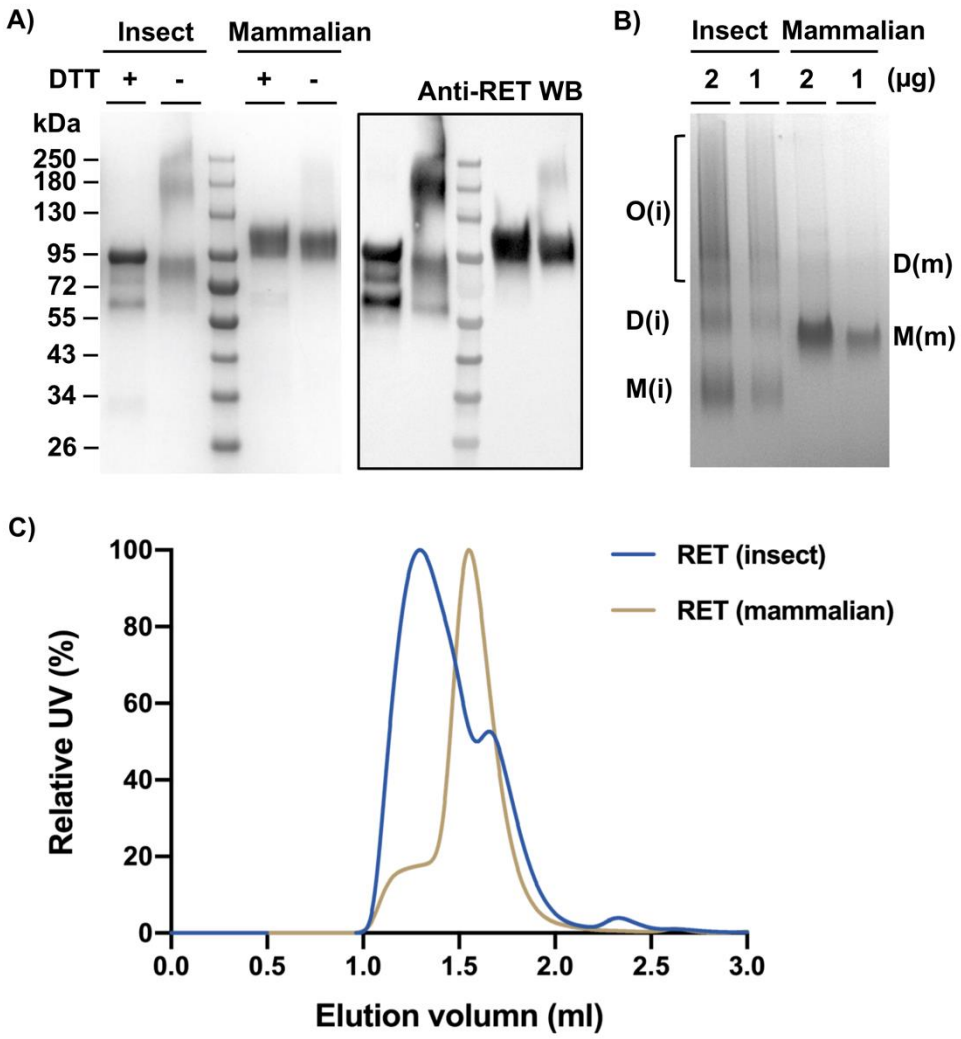

International Journal of Biological Macromolecules, Liu et al. Fig.3

A)

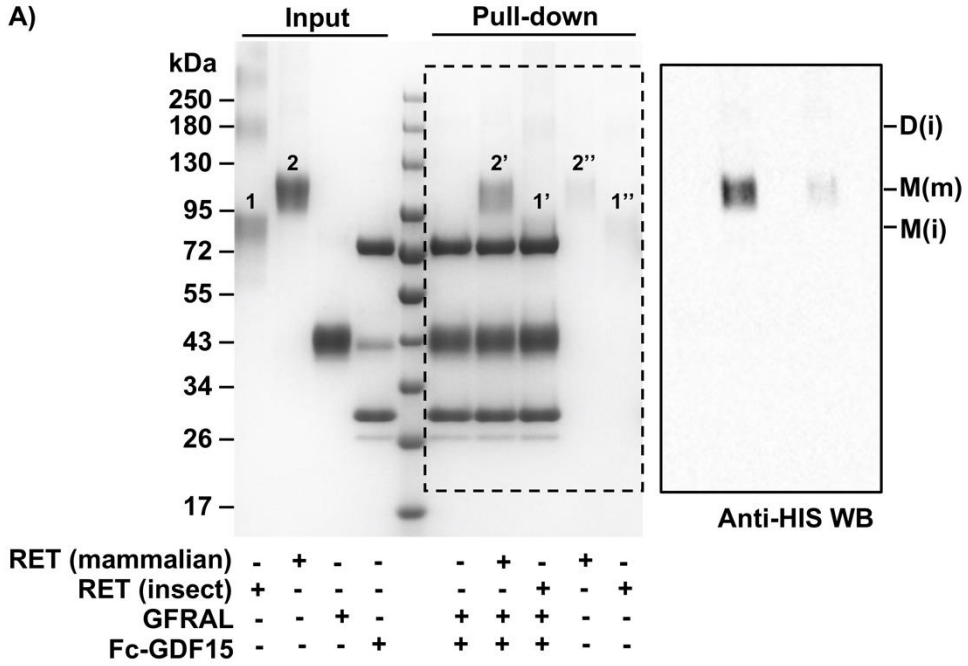

B)

	RET (insect)			RET (mammalian)		
Band No. (n)	1	1'	1''	2	2'	2''
Area ($U/1000$)	8.96	1.32	1.13	20.67	12.50	1.72
Activity* (%)	2.12			52.15		
*$Activity\ (\%) = \ (Un' - Un'')/Un \times 100\ (n = 1{,}2)$						

International Journal of Biological Macromolecules, Liu et al. Fig.4

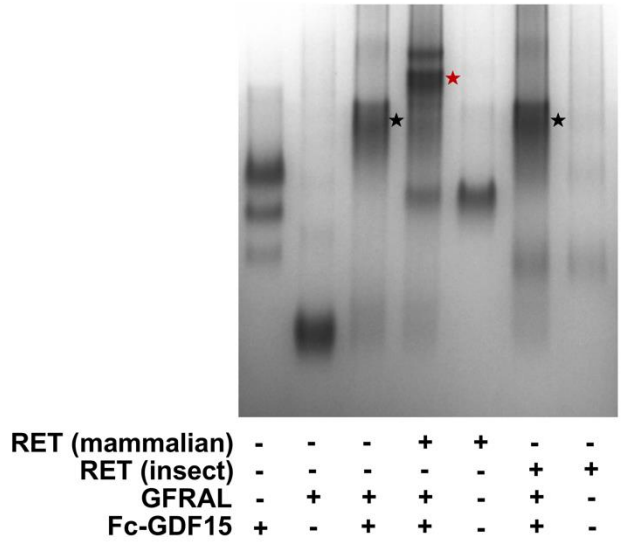

International Journal of Biological Macromolecules, Liu et al. Fig.5

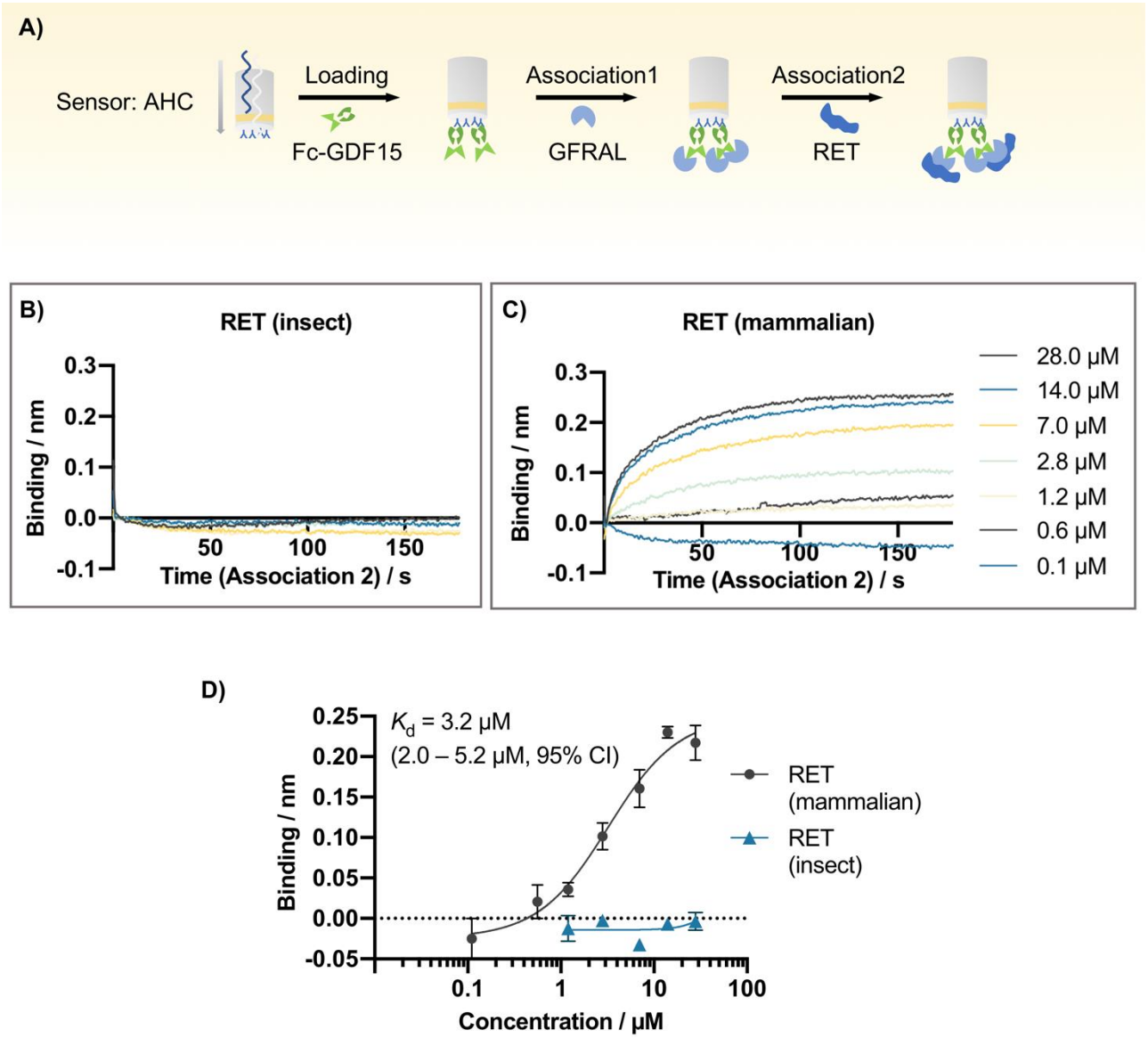

International Journal of Biological Macromolecules, Liu et al. Fig.6

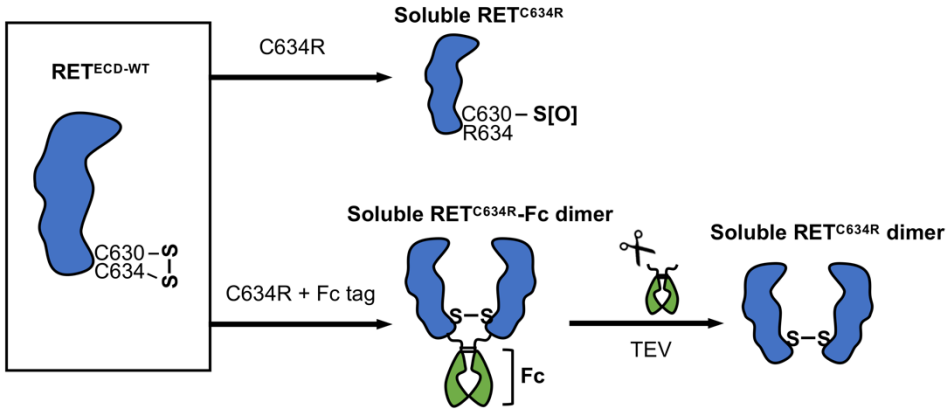

1

2 **International Journal of Biological Macromolecules, Liu et al. Fig.7**

3

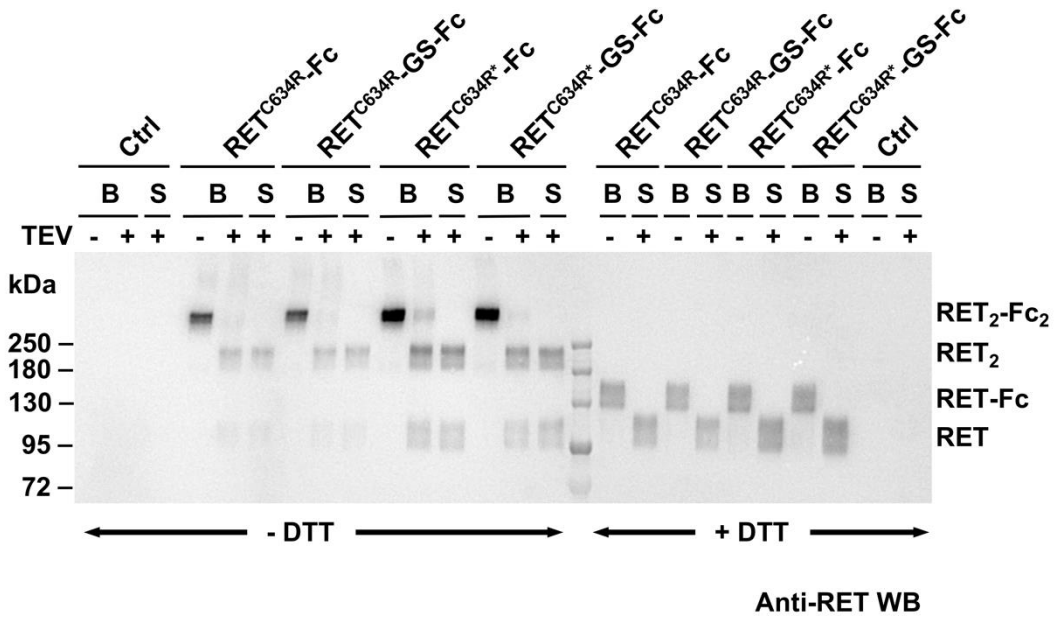

International Journal of Biological Macromolecules, Liu et al. Fig.8

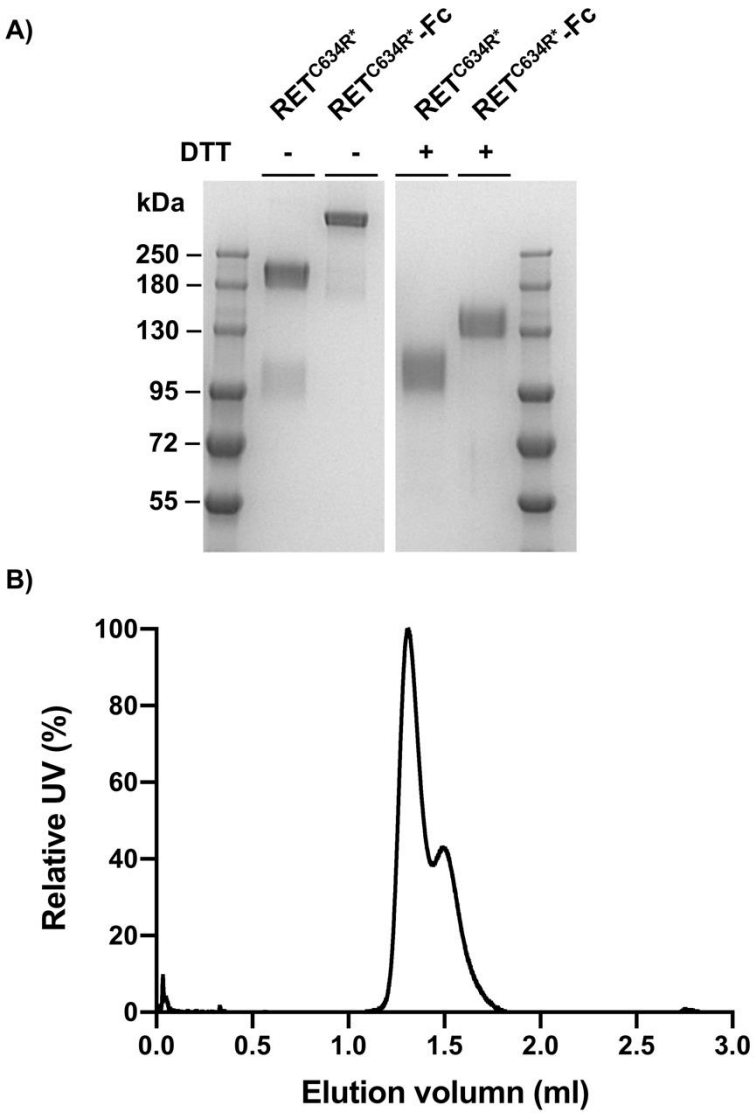

1

2

3 **International Journal of Biological Macromolecules, Liu et al. Fig.9**

Supplementary Information

Pull-down assays

Comparing the activity of RET^{ECD} expressed using CHO-K1 and HEK293T cells

In brief, RET^{ECD} expressed using either CHO-K1 or HEK293T cells was added to pre-incubated Fc-GDF15/GFRAL mixture and the final concentration of RET^{ECD}, GFRAL and Fc-GDF15 was 2.5 μM, 2.5 μM and 1.25 μM, respectively. After 1-hr incubation at 4 ˚C, 5 μl protein A resin was added to each sample together with 400 μl binding buffer and the samples were mixed by end-to-end rotation for 2 hr at 4 ˚C. The resin was then washed and incubated with SDS PAGE loading buffer without DTT before electrophoresis.

RET^{ECD} mutants and their binding to GDF15/GFRAL

Single mutations of RET^{ECD} (N336Q, N343Q and N468Q) were introduced using Q5 site directed mutagenesis. The soluble ECDs of RET^{N336Q}, RET^{N343Q} and RET^{N468Q} were expressed as described earlier for the wild-type RET^{ECD} and purified by Ni-NTA affinity chromatography. Pull-down assay was performed as described earlier and samples were analysed under non-reducing conditions using Coomassie-stained SDS-PAGE gel.

Deglycosylation

5 μg of RET^{ECD} (insect) was deglycosylated using Endo H_f or PNGase F under native and denaturing conditions according to the manufacturer's protocol. Phenylmethylsulfonyl fluoride (PMSF) was supplemented to all samples at a final concentration of 1 mM to prevent possible proteolysis. After the addition of the glycosidases, the mixture was incubated at 37 ˚C for 1 hr under denaturing conditions and 4 hr under native conditions. Afterwards, the samples were mixed with SDS PAGE loading buffer with DTT and were subject to electrophoresis.

Western blotting

For western blotting, proteins were transferred to 0.2 μm nitrocellulose membrane with the Trans-Blot Turbo transfer system and membranes were blocked with 3% BSA in TBST for 30 min. After being probed with appropriate antibodies, the membranes were washed three times in TBST, developed with enhanced

chemiluminescence (ECL) substrate and imaged using a ChemiDoc XRS+ System (Bio-Rad) to detect bound antibodies. Anti-RET(C-3)-HRP conjugated antibody was used at 1:1000 dilution in blocking buffer. Anti-5xHIS antibody was used at 1:5000 dilution in blocking buffer and horseradish peroxidase (HRP) conjugated mouse IgG kappa binding protein (m-IgGκ BP-HRP) secondary antibody was used at 1:5000 dilution in 10% non-fat milk dissolved in TBS.

Supplementary Table 1. *Approaches used to express RET^{ECD} using mammalian cells.*

Target protein	**Construct**	**Vector**	**Cell line**	**Expression method**	**Reference**
humanRET^{ECD} (amino acids 1-635)	RET-TEV-Protein A	pcDNA3	CHO Lec8	Stable cell line	[15]
	RET-HA-c-Myc-His_6	pSecTag2AHA	CHO	Stable cell line	[20]
	RET-TEV-His_6	/	CHO	Transient	[17]
	RET-His_8	pEZT-BM	HEK293S GnTI- or FreeStyle 293 F cells	Transient (Baculoviruses)	[16]
	RET-TEV-His_8-Flag	pcDNA3	HEK293T	Transient	(This study)
humanRET^{ECD} (amino acids 29-635)	RET-Fc RET-His	pJSV (CD33 signal peptide)	HEK293 6E cells	Transient	[11]

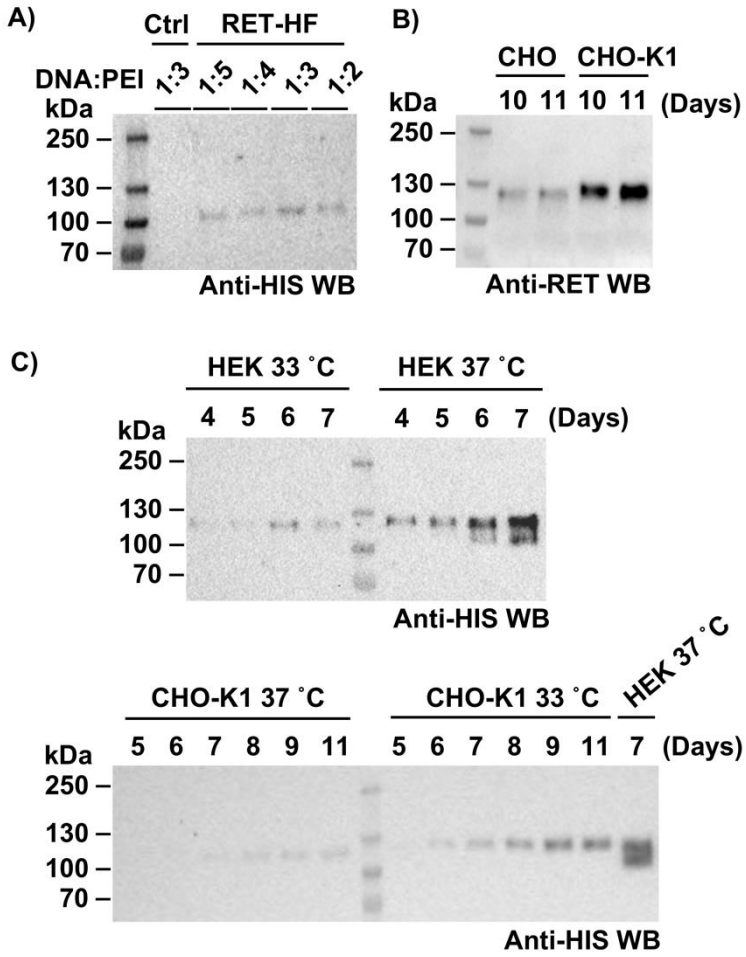

Supplementary Figure 1. Western blot images showing RET^{ECD} expression using HEK293T, CHO-K1 and CHO cells under various conditions. **A**) The expression of RET^{ECD} in HEK293T cells transfected using different DNA:PEI ratios; **B**) The expression of RET^{ECD} in CHO and CHO-K1 cells 10- or 11-day post-transfection at 33 ˚C. **C**) Time dependent expression of RET^{ECD} using HEK293T and CHO-K1 cells at 33 ˚C and 37 ˚C.

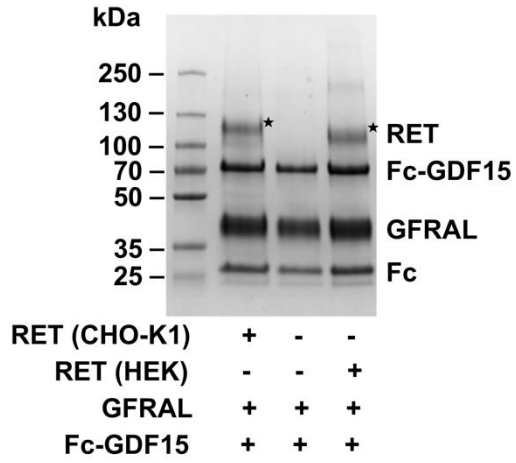

Supplementary Figure 2. Coomassie-stained SDS PAGE gel image showing RET^{ECD} expressed in CHO-K1 and HEK293T cells pulled down by GDF15/GFRAL. RET pulled down is marked with a star. All samples were treated with SDS loading dye without DTT.

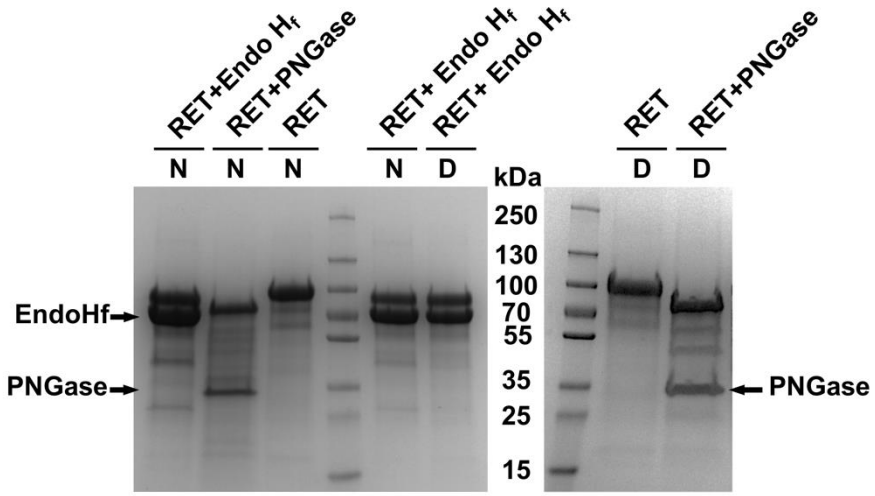

Supplementary Figure 3. Deglycosylation of RET^{ECD} (insect) by Endo H_f and PNGase F under native and denaturing conditions. Non-treated RET^{ECD} has a MW of 95kDa while the calculated MWs of RET^{ECD} treated by EndoHf and PNGase are 90 and 75 kDa, respectively. All samples are treated with SDS loading dye with DTT for electrophoresis. N: Native condition; D: Denaturing condition.

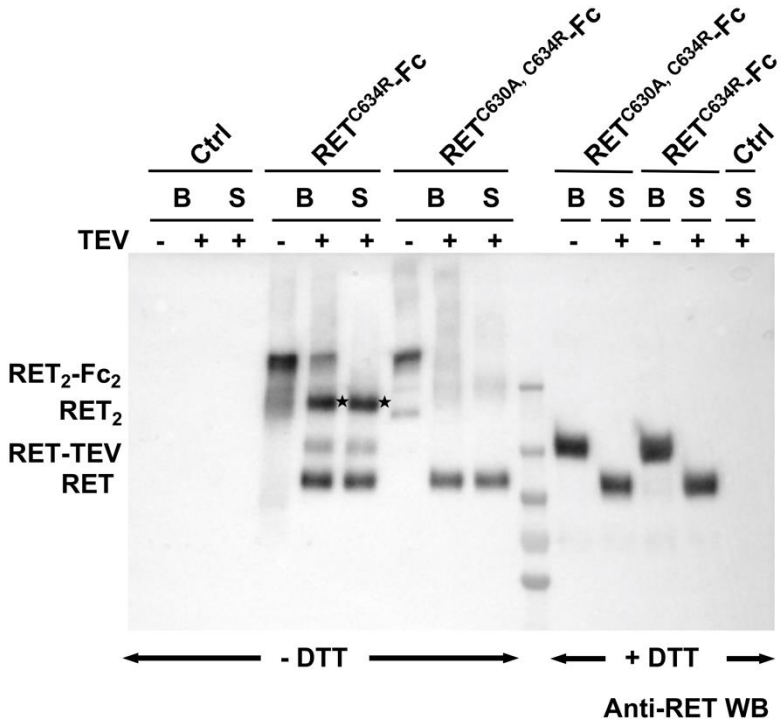

Supplementary Figure 4. Anti-RET WB showing the expression of RET^{C634R}-Fc, $RET^{C630A,C634R}$-Fc and RET^{C634R} dimer after Fc tag removal (marked by the black stars). Samples were prepared under non-reducing (- DTT) and reducing conditions (+ DTT). B: Protein A beads; S: Supernatant sample after spinning down the beads.

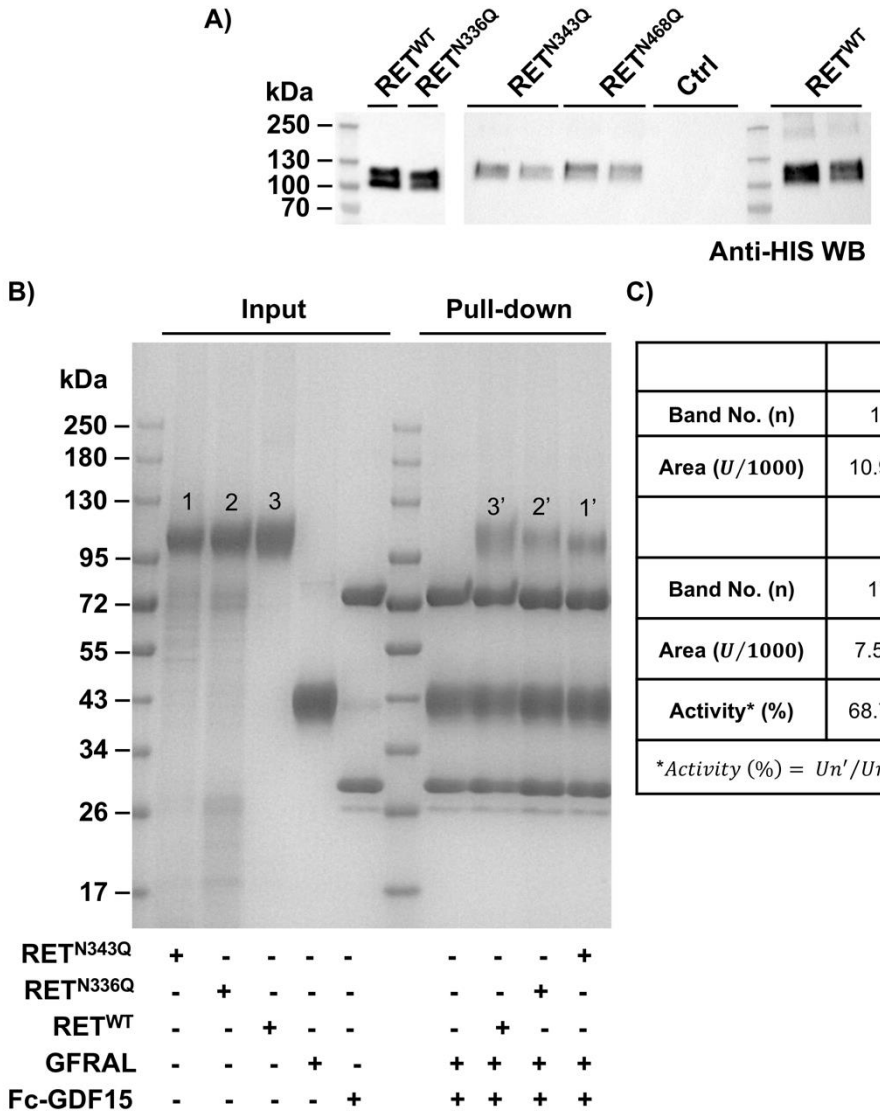

C)

	Input		
Band No. (n)	1	2	3
Area ($U/1000$)	10.96	13.73	14.82
	Pull-down		
Band No. (n)	1'	2'	3'
Area ($U/1000$)	7.53	6.58	8.24
Activity* (%)	68.70	47.92	55.60
*$Activity\ (\%) = Un'/Un \times 100\ (n = 1,2,3)$			

Supplementary Figure 5. Expression of RET^{ECD} mutants in HEK293T cells and their binding to GDF15/GFRAL. All samples are treated with SDS loading dye without DTT. **A**) Anti-HIS western blot showing the expression of different RET^{ECD} mutants N336Q, N343Q and N468Q. Expression was done in duplicates. **B**) Coomassie-stained gel image showing the protein A resin pull down of different RET^{ECD} mutants by Fc-GDF15/GFRAL. **C**) The table shows the band intensity as measured by ImageJ (Area (U)). Bands correspond to the wild-type RET^{ECD} and mutants are labelled (1 for N343Q, 2 for N336Q and 3 for wild-type). U: units.